Cellular/Molecular

Molecular Mechanisms Contributing to TARP Regulation of Channel Conductance and Polyamine Block of Calcium-Permeable AMPA Receptors

David Soto,[1] Ian D. Coombs,[2] Esther Gratacòs-Batlle,[1] Mark Farrant,[2] and Stuart G. Cull-Candy[2]

[1]Laboratory of Neurobiology, Bellvitge Biomedical Research Institute, 08907 L'Hospitalet de Llobregat, Spain, and [2]Department of Neuroscience, Physiology and Pharmacology, University College London, London WC1E 6BT, United Kingdom

Many properties of fast synaptic transmission in the brain are influenced by transmembrane AMPAR regulatory proteins (TARPs) that modulate the pharmacology and gating of AMPA-type glutamate receptors (AMPARs). Although much is known about TARP influence on AMPAR pharmacology and kinetics through their modulation of the extracellular ligand-binding domain (LBD), less is known about their regulation of the ion channel region. TARP-induced modifications in AMPAR channel behavior include increased single-channel conductance and weakened block of calcium-permeable AMPARs (CP-AMPARs) by endogenous intracellular polyamines. To investigate how TARPs modify ion flux and channel block, we examined the action of γ-2 (stargazin) on GluA1 and GluA4 CP-AMPARs. First, we compared the permeation of organic cations of different sizes. We found that γ-2 increased the permeability of several cations but not the estimated AMPAR pore size, suggesting that TARP-induced relief of polyamine block does not reflect altered pore diameter. Second, to determine whether residues in the TARP intracellular C-tail regulate polyamine block and channel conductance, we examined various γ-2 C-tail mutants. We identified the membrane proximal region of the C terminus as crucial for full TARP-attenuation of polyamine block, whereas complete deletion of the C-tail markedly enhanced the TARP-induced increase in channel conductance; thus, the TARP C-tail influences ion permeation. Third, we identified a site in the pore-lining region of the AMPAR, close to its Q/R site, that is crucial in determining the TARP-induced changes in single-channel conductance. This conserved residue represents a site of TARP action, independent of the AMPAR LBD.

Key words: **AMPA receptors; calcium-permeable AMPARs; channel conductance; polyamine block; TARP action; TARPs**

Introduction

Most fast excitatory synaptic transmission in the brain is mediated by AMPA-type glutamate receptors (AMPARs). Differences in AMPAR subunit composition contribute greatly to the diversity of glutamatergic synaptic signaling (Traynelis et al., 2010). AMPARs that lack the GluA2 subunit are characterized by permeability to calcium ions (Geiger et al., 1995), and regulation of this important class of receptors is thought to underlie a variety of physiological and pathological changes at central synapses (Cull-Candy et al., 2006; Isaac et al., 2007).

Functionally, calcium-permeable AMPARs (CP-AMPARs) are readily distinguished from calcium-impermeable subtypes, in that they display a high single-channel conductance (Swanson et al., 1997) and strong inward rectification conferred by endogenous intracellular spermine (Cull-Candy et al., 2006; Bats et al., 2012; but see Bowie, 2012). The calcium permeability of AMPARs depends critically on the presence of a neutral glutamine residue at the Q/R site in the inner vestibule of the channel at the selectivity filter. Of the AMPAR subunits, only GluA2 is edited at this site, with the glutamine being replaced by a positively charged arginine (Seeburg and Hartner, 2003). This renders GluA2-containing AMPARs impermeable to calcium ions and insensitive to block by intracellular polyamines.

AMPAR properties are also critically dependent on the presence of auxiliary transmembrane proteins (Coombs and Cull-Candy, 2009; Jackson and Nicoll, 2011). Of these, transmembrane AMPAR regulatory proteins (TARPs) are probably the best characterized. The prototypical TARP, stargazin (γ-2) is

Received Jan. 28, 2014; revised June 19, 2014; accepted July 15, 2014.

Author contributions: D.S., I.D.C., E.G.-B., M.F., and S.G.C.-C. designed research; D.S., I.D.C., and E.G.-B performed research; D.S., I.D.C., E.G.-B., M.F., and S.G.C.-C. analyzed data; D.S., I.D.C., M.F., and S.G.C.-C. wrote the paper.

This work was supported by the Spanish Ministry of Science and Technology cofunded with European Union funds (European Regional Development Fund Grant BFU2011-24725; D.S.), European Commission (FP7-PEOPLE-2011-CIG) Grant 293498 (D.S.), Government of Catalonia Grant SGR 2009-152, Wellcome Trust Grant 086185/Z/08/Z (S.G.C.-C. and M.F.), and Medical Research Council Grants MR/J002976/1 (S.G.C.-C. and M.F.) and MR/J012998/1 (M.F. and S.G.C.-C.). D.S. was supported by "Ramón y Cajal" Programme Grant RYC-2010-05970. We thank Raquel Yustos (Imperial College, London, UK) and Dr. Pau Gorostiza (Institute for Bioengineering of Catalonia, Barcelona, Spain) for providing us with tsA201 cells, and members of the Cull-Candy/Farrant laboratory for help and discussions.

This article is freely available online through the *J Neurosci* Author Open Choice option.

Correspondence should be addressed to the following: David Soto, Laboratori de Neurobiologia, Institut d'Investigació Biomèdica de Bellvitge, Feixa Llarga s/n, 08907 L'Hospitalet de Llobregat, Spain, E-mail: dsoto@idibell.cat; Mark Farrant, Department of Neuroscience, Physiology and Pharmacology, University College London, Gower Street, London WC1E 6BT, UK, E-mail: m.farrant@ucl.ac.uk; or Stuart Cull-Candy, Department of Neuroscience, Physiology and Pharmacology, University College London, Gower Street, London WC1E 6BT, UK, E-mail: s.cull-candy@ucl.ac.uk

DOI:10.1523/JNEUROSCI.0383-14.2014

Copyright © 2014 Soto et al.

This is an Open Access article distributed under the terms of the Creative Commons Attribution License (http://creativecommons.org/licenses/by/3.0), which permits unrestricted use, distribution and reproduction in any medium provided that the original work is properly attributed.

known to slow channel deactivation and desensitization (Nicoll et al., 2006) and to greatly increase single-channel conductance (Tomita et al., 2005; Soto et al., 2007). Furthermore, its presence markedly attenuates the block of CP-AMPARs by intracellular polyamines while enhancing their sensitivity to extracellular philanthotoxin-433 (Jackson et al., 2011) and increasing their permeability to calcium ions (Kott et al., 2009; Coombs et al., 2012). Despite the critical importance of these various features in shaping synaptic transmission, it remains unclear how TARP interaction regulates CP-AMPAR channel properties.

The reduction in polyamine block of CP-AMPARs conferred by TARPs could reflect a modification in pore size or structure, resulting in a decrease in binding site affinity for spermine or a reduced access to a binding site (Milstein and Nicoll, 2008; Bowie, 2012). Alternatively, associated TARPs could alter the local charge environment, thereby influencing ion flux or polyamine block. Positively charged residues located immediately proximal to the transmembrane domain of auxiliary kainate receptor (KAR) subunits Neto1 and Neto2 attenuate polyamine block and inward rectification of CP-KARs (Fisher and Mott, 2012). A corresponding region in the intracellular C-tail of TARPs is also rich in positive residues (Chu et al., 2001), raising the possibility that the TARP C-tail plays a role in attenuating polyamine block. Furthermore, the AMPAR subunits themselves have a conserved negative charge at the +4 position (relative to the Q/R site), the replacement of which has been shown to greatly decrease polyamine block of CP-AMPARs (Panchenko et al., 1999), suggesting that residues close to the selectivity filter may be involved in polyamine binding.

We investigated the relation between TARPs, ion flux, and polyamine block of CP-AMPARs. Our experiments indicate that TARPs increase the permeability of large organic cations but not the pore size of CP-AMPARs. Furthermore, we find that the C-tail of the TARP directly affects channel conductance and polyamine block and that a conserved negative residue in the pore (Q/R +4) plays a critical role in the TARP modulation of channel conductance.

Materials and Methods

Heterologous expression. We expressed recombinant AMPAR subunits and TARPs in tsA201 cells. AMPAR subunit cDNAs were a gift from S. Heinemann (Salk Institute, La Jolla, CA) and P. Seeburg (Max Planck Institute, Heidelberg, Germany), and γ-2, γ-3, and γ-5 were gifts from R. Nicoll (University of California, San Francisco, San Francisco, CA). All cDNAs were rat. Cell lines were maintained under standard protocols as described previously (Soto et al., 2007). Transient transfection was performed with either Lipofectamine 2000 (Invitrogen) or Gene Juice (Merck Millipore), according to the directions of the manufacturers. In all transfections, the total amount of DNA was 0.8 μg. Cells were split 12–24 h after transfection and plated on glass coverslips in the presence of 50 μM NBQX (Tocris-Abcam) to avoid AMPAR-mediated toxicity. Electrophysiological recordings were performed 24–48 h later.

AMPAR subunit and γ-2 molecular biology. Based on the predicted transmembrane domains of γ-2 (Chu et al., 2001), the C-terminal domain of γ-2 was analyzed. Three positively charged residues close to the fourth post-transmembrane domain were identified. The C-terminal domain of γ-2 begins at amino acid position D203 as follows: DRHKQLRAT… The positively charged residues R204, H205, and K206 were mutated to the noncharged residues serine (R204S) or asparagine (H205N, K206N). The triple mutant (R204S + H205N + K206N) was also generated. To create the point mutations D586N and D586K at position +4 from the Q/R site in the GluA1 AMPAR subunit, we performed site-directed mutagenesis using the same strategy. Additionally, the C-tail was deleted by introducing stop codons at position 206 or 229 (γ-2ΔC and $\gamma\text{-}2_{(1-228)}$, respectively). For this, we used either the Quickchange II site-directed mutagenesis kit (catalog #200523; Agilent Technologies) or Phusion polymerase (Finnzymes). In general, changes were incorporated using overlapping mismatched primers except for GluA1(D586K), which was created using abutting phosphorylated primers and subsequent ligation (Rapid Ligation Kit; Roche), and γ-2ΔC, for which we used the Quickchange method. The γ-2/6 chimera was created by amplifying, digesting, and then ligating the γ-2 N-terminal regions (including pIRES vector) and the γ-6 C-tail. A point mutation incorporated by the cloning process was corrected to give the final sequence. GluA1–γ-2 tandems were created by incorporating a 9 aa linker (GluA1-GGGGGEFAT-γ-2). The primers used are shown in Table 1.

Table 1. Primer sequences used in the study

Construct	Primer sequence
R204S	
Forward	CATGTTTATCGACAGCCACAAACAG
Reverse	GCTGTTTGTGGCTGTCGATAAACAT
H205N	
Forward	GTTTATCGACCGCAACAAACAGCTG
Reverse	CAGCTGTTTGTTGCGGTCGATAAAC
K206N	
Forward	GACCGCCACAATCAGCTGC
Reverse	GCAGCTGATTGTGGCGGTC
R204S + H205N + K206N	
Forward	AGCAACAATCAGCTGCGGG
Reverse	CCCGCAGCTGATTGTTGCT
GluA1(D586N)	
Forward	CAGCAAGGATGTAACATTTCCCCCAG
Reverse	CTGGGGGAAATGTTACATCCTTGCTG
GluA1(D586K)	
Forward	pATTTCCCCCAGGTCCC
Reverse	pTTTACATCCCTGCTGCA
ΔC terminus	GTTTATCGACCGCCACTAACAGCTGCGGGCC
γ-2(1–228)	
Forward	CATCCCCAGCTAGCGCTACCG
Reverse	CGGTAGCGCTAGCTGGGGATG
γ-2/6	
γ-2 Forward	GCACATGTTTATCGCGAACCGCCACAAACAGC
γ-2 Reverse	GCTGTTTGTGGCGGTTCGCGATAAACATGTGC
γ-6 Forward	CACTGCCTTCCTGGCCCTGGG
γ-6 Reverse	GGCGGATCCGAGTCGAGCTAG
Final mutagenesis	GTGCACATGTTTATCACACTGCCTTCCTGG
GluA1 tandems	
Forward	TTTTTGCTAGCATGCCGTACATCTTTGCC
Reverse	TTTTGAATTCTCCTCCTCCTCCAATTTTAACACTCTCGATG

Electrophysiology: general procedures. Cells were visualized with a fixed-stage upright or an inverted microscope (BX51 WI or IX50; Olympus). Electrodes were fabricated from borosilicate glass (1.5 mm outer diameter, 0.86 mm inner diameter; Harvard Apparatus) pulled with a PC-10 vertical puller (Narishige) and had a final resistance of 7–14 MΩ. Macroscopic currents were recorded at room temperature (22–25°C) from outside-out patches excised from GFP-positive cells. Currents were recorded with Axopatch 200A or 200B amplifiers, filtered at 10 kHz, and digitized at 50 kHz using Digidata 1200 or 1440A interfaces with pClamp 10 software (Molecular Devices).

Recording solutions. For rectification experiments and nonstationary fluctuation analysis (NSFA), the extracellular solution contained the following (in mM): 145 NaCl, 2.5 KCl, 1 $CaCl_2$, 1 $MgCl_2$, 10 glucose, and 10 HEPES, pH 7.3 with NaOH. For fast agonist application, 10 mM glutamate was added to the extracellular solution. The intracellular solution contained the following (in mM): 145 CsCl, 2.5 NaCl, 1 Cs-EGTA, 4 MgATP, and 10 HEPES, pH 7.2 with CsOH. Spermine tetrahydrochloride (Tocris Bioscience or Sigma-Aldrich) was added to intracellular solution at 100 μM. In experiments aimed to calculate the permeability for organic cations relative to Cs^+, the intracellular solution in all conditions contained the following (in mM): 140 CsCl, 5 Cs-EGTA, and 10 HEPES, pH 7.2 with CsOH. Spermine was not included because this enabled us to resolve the reversal potential more clearly.

The control Cs^+ extracellular solution contained the following (in mM): 140 CsCl, 10 glucose, and 10 HEPES. Test solutions were chloride salts of test organic cations at 140 mM. We used the following cations: methylamine (MA), dimethylamine (DMA), tetramethylammonium (TMA), tetraethylammonium (TEA), and *N*-methyl-D-glucamine (NMDG). In these experiments, spermine was not added to the intracellular solution to reduce rectification and to allow a better determination of the reversal potential. Cyclothiazide (CTZ; Tocris-Abcam) at 5 μM was added to limit desensitization of AMPARs.

Agonist application to excised patches. Rapid agonist application was achieved by switching between a continuously flowing control solution (extracellular solution diluted by 4%) and a glutamate-containing solution (extracellular solution plus 2.5 mg/ml sucrose and 10 mM glutamate). Solution switching was achieved by piezoelectric translation of a theta-barrel application tool made from borosilicate glass (2 mm outer diameter from Hilgenberg or 1.5 mm outer diameter from Sutter Instruments) mounted on a piezoelectric translator (P-265.00 or P-601.30; Physik Instrumente). One hundred or 200 ms jumps were applied to outside-out patches at different potentials (10 or 20 mV steps). At the end of each experiment, the adequacy of the solution exchange was tested by destroying the patch and measuring the liquid-junction current at the open pipette (10–90% rise time typically 250 μs). For pore size determination experiments, rapid pulses of glutamate (100 ms; 1 mM in the presence of 5 μM CTZ) were applied to outside-out patches at different potentials (5 mV steps), and the glutamate-evoked peak currents were plotted at each voltage for each cation. In this way, we were be able to determine the reversal potential for the different cations.

Rectification index. The rectification index (RI) was defined as the absolute value of the average peak response at +40 mV divided by that at −80 mV:

$$RI_{+40\ \mathrm{mV}/-80\ \mathrm{mV}} = |I_{+40\ \mathrm{mV}}|/|I_{-80\ \mathrm{mV}}|. \quad (1)$$

In this case, a linear current–voltage (*I–V*) relationship would yield an RI of 0.5.

Kinetics of AMPAR-mediated responses. For the determination of the kinetics of desensitization of the glutamate-activated currents, we performed fits to a double-exponential function to calculate the weighted time constant ($\tau_{w,des}$) according to the following:

$$\tau_{w,des} = \tau_f\left(\frac{A_f}{A_f + A_s}\right) + \tau_s\left(\frac{A_s}{A_f + A_s}\right), \quad (2)$$

where A_f and τ_f are the amplitude and time constant of the fast component of desensitization, and A_s and τ_s are the amplitude and time constant of the slow component of desensitization.

Conductance–voltage relationships. The relationship between the normalized conductance and voltage was fitted by the Boltzmann equation:

$$G = G_{max}\left(\frac{1}{1 + \exp((V_m - V_{1/2})/k)}\right), \quad (3)$$

where G_{max} is the conductance at a sufficiently hyperpolarized potential to produce full relief of polyamine block, V_m is the membrane potential, $V_{1/2}$ is the potential at which 50% of block occurs, and k is a slope factor describing the voltage dependence of block.

Relative cation permeability. The permeability ratio for a given cation X^+ relative to Cs^+ (P_X/P_{Cs}) was calculated using the Goldman–Hodgkin–Katz equation for a cation-selective channel:

$$\frac{P_X}{P_{Cs}} = \left(\frac{[Cs^+]_i}{[X^+]_o}\right)\exp\left(\frac{FV_{rev}}{RT}\right), \quad (4)$$

where V_{rev} is the reversal potential, and $[X^+]_o$ and $[Cs^+]_i$ are the concentrations of the cations X^+ and Cs^+, where the subscripts o and i refer to extracellular and intracellular, respectively. *F*, *R*, and *T* have their usual values.

Estimation of the pore size. To estimate the diameter of the channel pore, we assumed that each cation X^+ was a sphere of diameter d_X and that the pore, at its narrowest point, was approximated by a cylinder of diameter d_{pore}. According to the "excluded volume" theory (Dwyer et al., 1980; Cohen et al., 1992), the permeability of an ion is proportional to the area of the narrowest region of the pore left unoccupied by the ion, and the relationship between relative permeability and ionic diameter is given by the following equation:

$$\sqrt{\frac{P_X}{P_{Cs}}} = a - b \times d_X, \quad (5)$$

where $a = d_{pore}/(d_{pore} - d_X)$ and $b = 1/(d_{pore} - d_X)$. We plotted the square root of the calculated permeability ratios for the ions (P_X/P_{Cs}) against their estimated geometric mean diameters (d_X) to obtain the slope (b) and intercept (a) (McKinnon et al., 2011). The diameter of the narrowest region of the pore is given by a/b. The ionic diameters were estimated as geometric mean diameters calculated from the dimensions (d_1, d_2, d_3) of the smallest box able to contain a space-filling molecular model of each ion (Burnashev et al., 1996), according to the following:

$$d_X = \sqrt[3]{d_1 \times d_2 \times d_3}. \quad (6)$$

The calculated diameters are given in Table 2.

Table 2. Permeability ratios (relative to Cs^+) for organic cations of different sizes

Ion	Ion size (nm)	Receptor	V_{rev} (mV)	P_X/P_{Cs}	*P* value
Cesium	0.346[a]	GluA1	0.44 ± 0.94 (7)	1.051 ± 0.043	0.26
		GluA1 + γ2	−1.82 ± 1.67 (7)	0.967 ± 0.056	
MA	0.376	GluA1	−2.83 ± 0.83 (5)	0.920 ± 0.030	0.27
		GluA1 + γ2	−4.52 ± 1.14 (5)	0.860 ± 0.040	
DMA	0.460	GluA1	−7.77 ± 1.65 (5)	0.758 ± 0.052	0.88
		GluA1 + γ2	−7.49 ± 2.16 (5)	0.772 ± 0.070	
TMA	0.550	GluA1	−30.76 ± 3.51 (5)	0.269 ± 0.040	0.043
		GluA1 + γ2	−23.00 ± 0.65 (4)	0.400 ± 0.011	
TEA	0.657	GluA1	−57.09 ± 1.26 (5)	0.081 ± 0.006	0.0002
		GluA1 + γ2	−46.69 ± 1.01 (5)	0.138 ± 0.007	
NMDG	0.727	GluA1	−90.60 ± 1.58 (4)	0.024 ± 0.002	0.041
		GluA1 + γ2	−85.78 ± 0.70 (5)	0.031 ± 0.001	

Currents were recorded from outside-out patches from tsA201 cells expressing GluA1 alone or GluA1 + γ-2, as indicated. V_{rev} refers to the 0 current potential for a given cation. The number of cells is indicated in parentheses. P_X/P_{Cs} was determined according to Equation 4 (see Materials and Methods). Each *p* value is from an unpaired Welch *t* test, comparing P_X/P_{Cs} values of GluA1 and GluA1 + γ-2. Ion sizes are geometric mean diameters corresponding to the dimensions of the smallest box that contains the ion as measured with Corey–Pauling–Koltum models, as described previously (Villarroel et al., 1995; Burnashev et al., 1996).

[a]*The cesium ion diameter is from Mähler and Persson (2012).*

NSFA. To deduce channel properties from macroscopic responses, glutamate (10 mM) was applied to outside-out patches (100 ms duration, 1 Hz, V_{hold} of −60 mV), and the ensemble variance of all successive pairs of current responses were calculated. The single-channel current (i) and the total number of channels in the patch (N) were determined by plotting this ensemble variance against mean current ($\bar{I}$) and fitting with a parabolic function:

$$\sigma^2 = \sigma_B^2 + \left(i\bar{I} - \left(\frac{\bar{I}^2}{N}\right)\right), \quad (7)$$

where σ^2_B is the background variance. Along with normal peak-to-peak variation in the currents attributable to stochastic channel gating, some patches presented a gradual reduction in peak amplitude. The mean response was calculated from the periods of the recordings showing stable responses that were identified using a Spearman's rank-order correlation test. The weighted-mean single-channel conductance was determined from the single-channel current and the holding potential corrected for the calculated liquid junction potential (+4.9 mV; pClamp 10).

Analysis and statistics. Recordings were analyzed using IGOR Pro (Wavemetrics) with NeuroMatic (J. Rothman, University College London, London, UK). Summary data are presented in the text as the mean ± SEM from *n* patches and in the figures as bar plots of the group mean, with error bars denoting the SEM. In the inset to Figure 1*F*, error bars denote 95% confidence intervals (CIs). Comparisons involving two

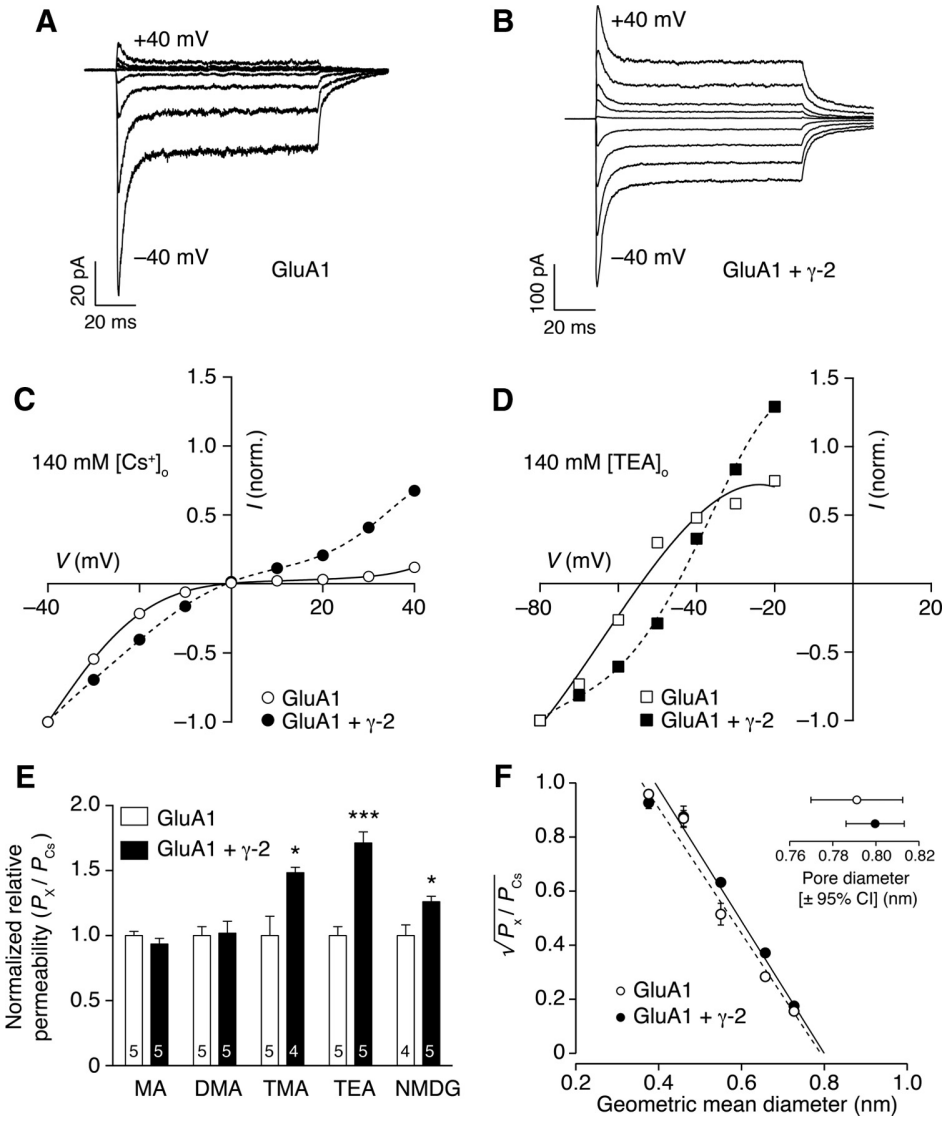

Figure 1. Estimates of the diameter of the narrowest pore constriction of GluA1 and GluA1 + γ-2. ***A***, Glutamate-evoked currents from homomeric GluA1 at different holding potentials between −40 and +40 mV (Δ10 mV) ($[CsCl]_{int}$ and $[CsCl]_{ext}$ both at 140 mM). Individual currents were activated by 100 ms applications of 1 mM glutamate plus 5 μM CTZ to an outside-out patch from a transfected tsA201 cell. Note that, even in the absence of added intracellular polyamines, some inward rectification remained. ***B***, Glutamate-evoked currents recorded in the same conditions as in ***A*** in a patch from a cell expressing GluA1 + γ-2. ***C***, *I–V* relationships constructed for the peak current responses shown in ***A*** and ***B***. ***D***, *I–V* relationships (−80 to −20 mV) for glutamate-evoked peak currents from cells expressing homomeric GluA1 and GluA1 + γ-2 in $TEA_{ext}/CsCl_{int}$ conditions. ***E***, Normalized permeability ratios of different organic cations relative to Cs^+ for GluA1 and GluA1 + γ-2 channels. Mean values and SEM are shown; numbers in columns denote the number of patches. No differences between GluA1 and GluA1 + γ-2 were found with MA and DMA, but differences were seen with TMA, TEA, and NMDG. $*p < 0.05$, $***p < 0.001$, unpaired two-tailed Welch *t* test. ***F***, Relationship between the permeability of organic cations relative to Cs^+ and their mean ionic diameter for GluA1 and GluA1 + γ-2. Symbols indicate mean values, and error bars denote ±SEM. The continuous and dashed lines are weighted fits to Equation 5 (see Materials and Methods), which gave the estimated pore diameters (and 95% CIs) shown in the inset.

datasets only were performed using a two-sided Welch two-sample *t* test. All analyses involving data from three or more groups were performed using one- or two-way ANOVA (Welch heteroscedastic *F* test), followed by pairwise comparisons using two-sided Welch two-sample *t* tests (with Holm's sequential Bonferroni correction for multiple comparisons). Differences were considered significant at $p < 0.05$. Statistical tests were performed using R (version 3.0.2; The R Foundation for Statistical Computing, http://www.r-project.org/) and RStudio (version 0.98.507; RStudio).

Results

γ-2 increases permeability but not pore size of CP-AMPARs

To determine whether the pore size of CP-AMPARs was influenced by the presence of an associated TARP, we examined the relative permeability of cations of different sizes (Villarroel et al., 1995; Burnashev et al., 1996). Specifically, we measured the reversal potential of glutamate-evoked currents in the presence of the organic cations MA^+, DMA^+, TMA^+, TEA^+, and $NMDG^+$ and estimated their permeability relative to that of the reference cation (Cs^+). We compared the reversal potentials of GluA1 receptors expressed with and without γ-2.

Currents were recorded from GluA1 and GluA1 + γ-2 at potentials from −40 to +40 mV in symmetrical solutions containing 140 mM CsCl (Fig. 1*A*,*B*). *I–V* relationships were constructed for the glutamate-evoked peak currents (Fig. 1*C*). The GluA1 responses showed limited rectification caused by residual endogenous spermine. Figure 1*D* illustrates a representative ex-

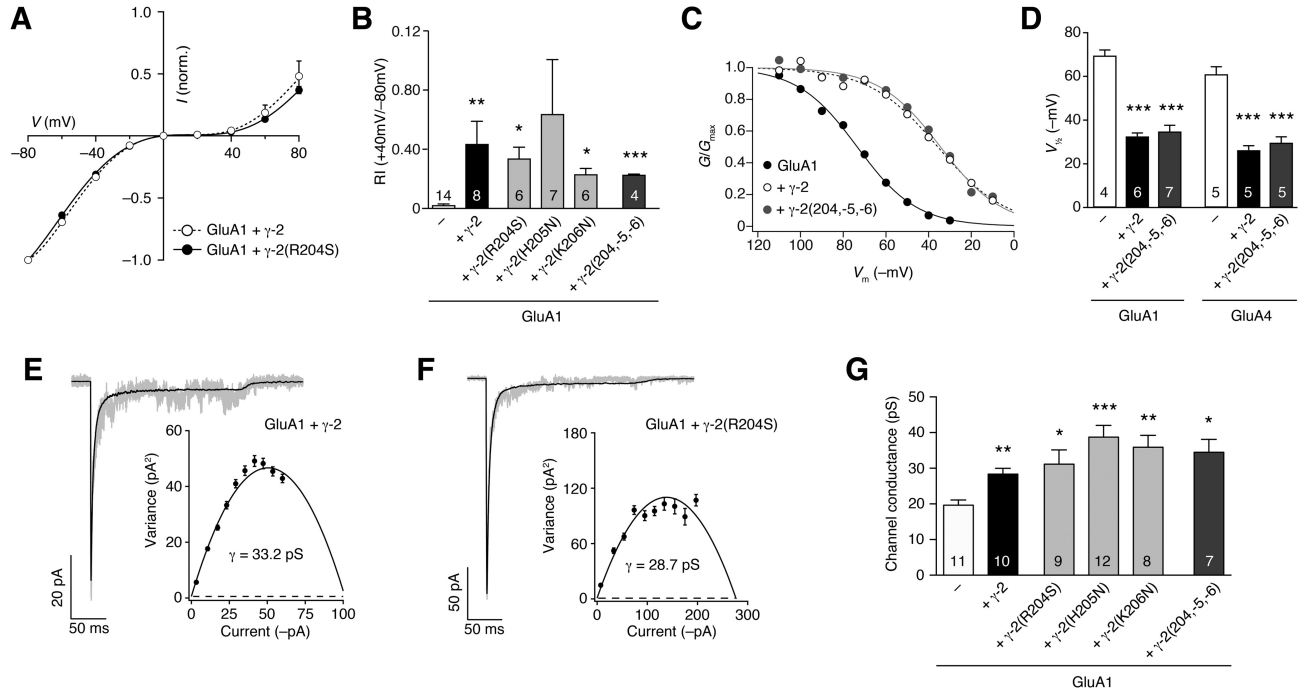

Figure 2. Mutations in the γ-2 C-tail do not affect polyamine block or channel conductance. ***A***, *I–V* relationships for peak glutamate-evoked (10 mM) responses recorded between −80 and +80 mV in outside-out patches from cells expressing GluA1 + wild-type γ-2 ($n = 4$) or GluA1 + γ-2(R204S) ($n = 4$). Error bars denote SEM. ***B***, Pooled data showing the RI (measured as the peak current at +40 mV/peak current at −80 mV) for GluA1 + γ-2 and mutated versions of γ-2. Mean values and SEM are shown; numbers in columns denote the number of patches. The RI differed across the six groups (one-way ANOVA, $F_{(8,14.5)} = 6.74$, $p < 0.001$). Differences between GluA1 alone and wild-type or mutant γ-2 are indicated (*$p < 0.05$, **$p < 0.01$, ***$p < 0.001$; unpaired Welch two-sample *t* tests with Holm's sequential Bonferroni correction). All mutants $p > 0.05$ compared with wild-type γ-2. ***C***, Representative normalized *G–V* relationships for peak glutamate-evoked (10 mM) responses recorded between −110 and −10 mV in three outside-out patches from cells expressing GluA1, GluA1 + wild-type γ-2, or GluA1 + γ-2(204, -5, -6). Lines are fits to a Boltzmann equation (Eq. 3; see Materials and Methods). For the examples shown, $V_{1/2}$ was shifted from −73.4 mV for GluA1 to −35.7 mV for GluA1 + wild-type γ-2 and to −34.4 mV for GluA1 + γ-2(204, -5, -6). ***D***, Pooled data showing $V_{1/2}$ values for GluA1 and GluA4 either alone or coexpressed with γ-2 or γ-2(204, -5, -6). Columns and error bars indicate mean values and SEM; numbers in columns denote the number of patches. Two-way ANOVA showed a significant main effect for the AMPAR ($F_{(1,26)} = 9.17$, $p < 0.01$), a significant main effect for TARP ($F_{(2,26)} = 90.37$, $p < 0.001$), and no significant interaction ($F_{(2,26)} = 0.14$, $p = 0.87$). ***$p < 0.001$, differences between GluA1 alone and wild-type and mutant γ-2 (unpaired Welch two-sample *t* tests with Holm's sequential Bonferroni correction). ***E***, Currents elicited by rapid application of 10 mM glutamate (200 ms) to an outside-out patch from a tsA201 cell (−60 mV) transfected with GluA1 + γ-2. A single raw trace (gray) is shown overlaid with the mean response (black). The inset shows the current–variance plot for the same recording. The fitted parabola (see Materials and Methods) gave a weighted single-channel conductance of 33.2 pS. Dashed line denotes background variance, and error bars denote SEM. ***F***, Same as in ***E*** but for a patch from a cell expressing GluA1 + γ-2(R204S); the fitted parabola gave a weighted mean single-channel conductance of 28.7 pS. ***G***, Pooled weighted mean single-channel conductance data from NSFA of GluA1 + wild-type and mutated versions of γ-2. Mean values and SEM are shown; numbers in bars denote the number of patches. Weighted mean conductance differed significantly across the six groups (one-way ANOVA, $F_{(8,26.7)} = 5.96$, $p < 0.001$). Multiple pairwise comparisons (unpaired Welch two-sample *t* tests with Holm's sequential Bonferroni correction) revealed differences between GluA1 alone and GluA1 expressed with wild-type or mutant γ-2 (*$p < 0.05$, **$p < 0.01$, ***$p < 0.001$). All mutants $p > 0.05$ compared with wild-type γ-2.

periment with TEA (mean diameter, 0.66 nm; Villarroel et al., 1995), in which there was a clear shift in the reversal potential with γ-2. Using the shift in reversal potential, we then calculated the relative permeability for each cation X^+ relative to Cs^+ according to the Goldman–Hodgkin–Katz equation for cation-selective channels (see Materials and Methods). When analyzed individually, we found that, for cations of relatively small diameter (MA and DMA), there was no detectable difference in reversal in the presence of γ-2 (Table 2), indicating no effect on the relative permeability of the channel (Fig. 1*E*). In contrast, the permeability of the larger cations TMA, TEA, and NMDG was increased when γ-2 was included (Fig. 1*E*; Table 2).

We obtained an estimate of the pore size by plotting the square root of the relative permeability against the diameter for organic cations. This analysis revealed that, whereas certain ions showed an increased relative permeability with γ-2, the estimated pore diameters for GluA1 alone and GluA1 + γ-2 were comparable. Thus, the pore diameters were 0.79 nm (95% CI = 0.77–0.81) for GluA1 alone and 0.80 nm (95% CI = 0.79–0.81) for GluA1 + γ-2 (Fig. 1*F*). This analysis suggests that the GluA1 pore diameter is not affected by γ-2. Thus, the marked reduction in polyamine block and the increase in channel conductance produced by γ-2 (and other auxiliary subunits; Soto et al., 2007, 2009; see Discussion) are unlikely to result from a simple increase in pore size. This change in ion permeability without an accompanying increase in pore diameter is in keeping with previous studies of both AMPARs and NMDARs, showing that ion selectivity and ion transport rate can be altered dramatically without a change in apparent pore size, at least at the selectivity filter (Burnashev et al., 1996; Wollmuth and Sakmann, 1998).

Do positive residues in the TARP C-tail mediate attenuation of polyamine block?

To determine whether the TARP C-tail influences ion flux, we first considered whether specific charged residues in the C-tail of γ-2 regulate polyamine block. Three positively charged residues (RKK) in the intracellular C-tail of the KAR-associated auxiliary subunits Neto1 and Neto2 are known to contribute to the attenuation of polyamine block of CP-KARs (Fisher and Mott, 2012). Therefore, we replaced similarly located positive charges in γ-2 (RHK) with neutral residues. Specifically, we created the point

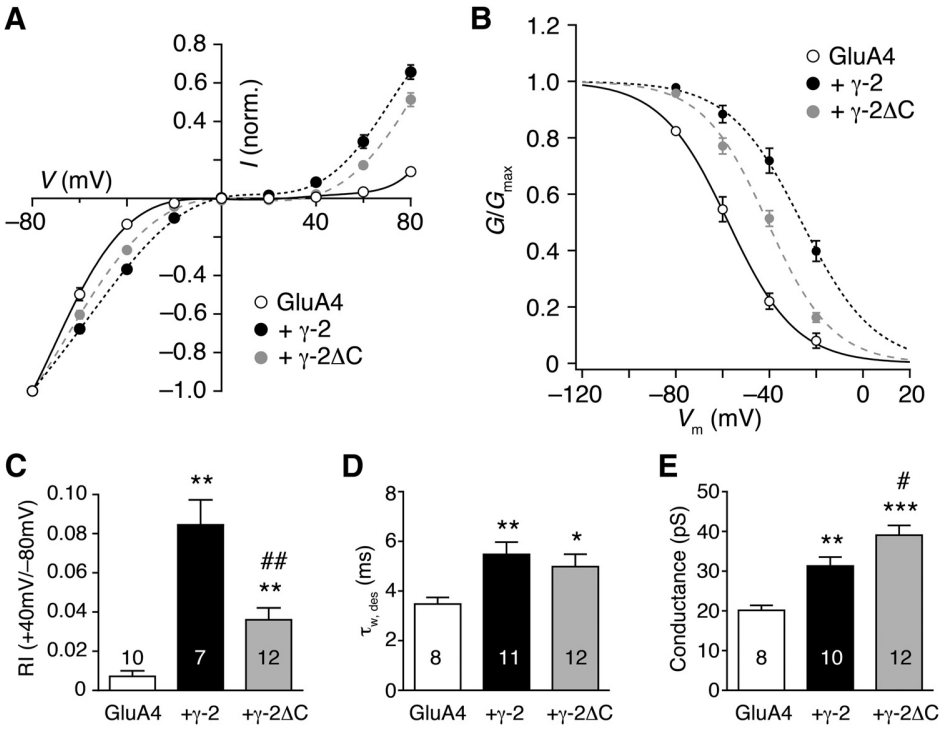

Figure 3. C-tail deletion of γ-2 modifies TARP effects on polyamine block and single-channel conductance. ***A***, *I–V* relationships for glutamate-evoked peak responses (10 mM) between −80 and +80 mV from outside-out patches expressing GluA4 homomers ($n = 10$), GluA4 + γ-2 ($n = 7$), and GluA4 + γ-2ΔC ($n = 12$). ***B***, Plot of normalized conductance against voltage (V_m) for GluA4 homomeric receptors alone or with γ-2 or γ-2ΔC. Data were obtained from records in ***A***. Lines are fits (at negative voltages) to a Boltzmann equation (see Materials and Methods). $V_{½}$ is shifted from −57.6 mV for GluA4 to −26.2 mV for GluA4 + γ-2 and to −40.8 mV for GluA4 + γ-2ΔC. ***C***, Pooled $RI_{+40/-80}$ values for GluA4 homomers alone or with γ-2 or γ-2ΔC. Mean values and SEM are shown; numbers in columns denote the number of patches. The RI differed across the three groups (one-way ANOVA, $F_{(2,12.06)} = 23.5$, $p < 0.001$). Multiple pairwise comparisons (unpaired Welch two-sample *t* tests with Holm's sequential Bonferroni correction) revealed significant differences between GluA1 alone and GluA1 expressed with wild-type or mutant γ-2 (**$p < 0.01$) and a significant difference between γ-2 and γ-2ΔC (##$p < 0.01$). ***D***, Pooled values of desensitization kinetics ($\tau_{w,des}$; details as for ***C***). Desensitization differed across the three groups ($F_{(2,18.22)} = 7.89$, $p < 0.01$). Multiple pairwise comparisons revealed differences between wild-type and mutant γ-2 compared with GluA1 alone (*$p < 0.05$, **$p < 0.01$) but no difference between γ-2 and γ-2ΔC. ***E***, Pooled values of weighted mean single-channel conductance (details as for ***C***). Channel conductance differed across the three groups ($F_{(2,17.42)} = 26.52$, $p < 0.001$). Multiple pairwise comparisons revealed differences between GluA1 alone and GluA1 expressed with wild-type or mutant γ-2 (**$p < 0.01$, ***$p < 0.001$) and a difference between γ-2 and γ-2ΔC (#$p < 0.05$).

mutations R204S, H205N, and K206N, as well as a triple mutant (see Materials and Methods). We applied glutamate to outside-out patches from cells transfected with GluA1 + γ-2 or GluA1 + mutants of γ-2 (Fig. 2*A*) and examined their effect on polyamine block by measuring the RI ($RI_{+40/-80}$; see Materials and Methods; Fig. 2*B*) and fitting conductance–voltage (*G–V*) relationships in the negative range (to determine $V_{½}$; see Materials and Methods; Fig. 2*C*,*D*). None of the mutations altered the γ-2-mediated reduction in polyamine block. This was also true for GluA4 (Fig. 2*D*). We next examined the γ-2-induced increase in the weighted mean single-channel conductance of GluA1, by performing NSFA (Fig. 2*E*,*F*). None of the mutations altered the γ-2-mediated increase in conductance (Fig. 2*G*). Together, our results suggest that these positive residues in the C-tail are not critical for γ-2 modulation of AMPAR channel properties.

Does the TARP C-tail play any role in the attenuation of polyamine block?

If positive residues in the γ-2 C-tail are not required, does the C-tail play any role in AMPAR channel modulation? To test this, we first examined the effect of deleting the entire C-tail (γ-2ΔC). These experiments were performed using homomeric GluA4 CP-AMPARs. We found that γ-2ΔC produced less relief of polyamine block than γ-2 (Fig. 3*A*,*B*). Thus, GluA4 + γ-2ΔC displayed greater rectification ($RI_{+40/-80}$; 0.036 ± 0.006, $n = 12$) than GluA4 + γ-2 (0.084 ± 0.013, $n = 7$), but less than GluA4 alone (0.007 ± 0.003, $n = 10$; Fig. 3*C*). $V_{½}$ was shifted from −57.6 to −26.2 mV by coexpression of γ-2 but was intermediate between these values with γ-2ΔC (−40.8 mV). This suggests that the C-tail of γ-2 does play a role in TARP modulation of AMPAR channel properties.

Does the effect of the C-tail truncation reflect a reduced interaction of AMPAR and TARP? AMPAR desensitization is known to be slowed by TARPs (Milstein and Nicoll, 2008), an effect mediated by their first extracellular loop (Tomita et al., 2005). Of note, γ-2 and γ-2ΔC were equally effective in slowing desensitization, increasing $\tau_{w,des}$ from 3.5 ± 0.3 to 5.5 ± 0.5 and 5.0 ± 0.5 ms, respectively ($n = 8$, 11, and 12; Fig. 3*D*). This suggests that GluA4 homomers are coassembled with γ-2 regardless of the presence or absence of the TARP C-tail.

Unexpectedly, we found that γ-2ΔC was more effective than full-length γ-2 at increasing the single-channel conductance of GluA4. The weighted mean channel conductance was 20.1 ± 1.3 pS for GluA4 alone, 31.3 ± 2.3 pS with γ-2, and 39.1 ± 2.5 pS with γ-2ΔC ($n = 8$, 10, and 12, respectively; Fig. 3*E*). Thus, the presence of a C-tail appears to limit the increase in single-channel conductance normally produced by coassembly with γ-2.

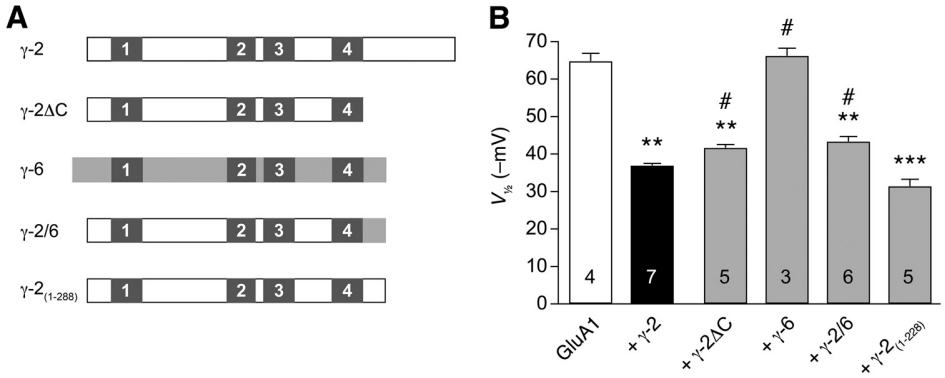

Figure 4. The proximal C-tail of γ-2 is necessary for maximal relief of polyamine block. ***A***, Diagram of the TARP constructs used. Numbered regions 1–4 represent the transmembrane domains. γ-2 is shown as white and γ-6 as light gray. $\gamma\text{-}2_{(1-228)}$ has an equivalent length of C terminus as γ-6. ***B***, Pooled data showing the voltage of half polyamine block ($V_{½}$) as derived from Boltzmann fits of *G–V* relationships recorded from GluA1 coexpressed with the constructs shown in ***A***. Mean values ± SEM are illustrated. The numbers in the columns denote the number of patches. $V_{½}$ differed across the six groups (one-way ANOVA, $F_{(5,8.72)} = 57.4$, $p < 0.001$). $^{**}p < 0.01$, $^{***}p < 0.001$, differences from GluA1 alone (unpaired Welch two-sample *t* tests with Holm's sequential Bonferroni correction). $V_{½}$ values with γ-2ΔC, γ-6, and γ-2/6 were different from those with wild-type γ-2 ($^{\#}p < 0.05$). $V_{½}$ values were not different between $\gamma\text{-}2_{(1-228)}$ and wild-type γ-2 or between γ-2ΔC and γ-2/6.

The proximal TARP C-tail contributes to the relief of polyamine block

To identify the region of the C-tail important for its contribution to TARP action and to establish whether the effects were seen with other AMPARs, we examined additional γ-2 truncation mutants using GluA1. With GluA1, γ-2ΔC produced less relief of polyamine block than did wild-type γ-2 ($V_{½}$ of −36.9 ± 0.6 mV with γ-2 and −41.7 ± 0.9 mV with γ-2ΔC, $n = 7$ and 5, respectively; Fig. 4*A*,*B*), although this was less marked than was seen with GluA4. Importantly, these changes appeared not to result from a reduced TARP stoichiometry, because we obtained similar results with GluA1–γ-2 tandem constructs that constrained AMPAR subunit:TARP stoichiometry (see Materials and Methods). Specifically, as with separately expressed subunits, we found that the polyamine block of GluA1–γ-2 was less than that of GluA1–γ-2ΔC ($V_{½}$ of −35.7 ± 1.9 and −40.6 ± 1.1 mV, $n = 8$ and 9, respectively; $p < 0.05$, Welch *t* test).

To confirm that the reduced effect of γ-2ΔC was not attributable to unexpected alterations in the gross structure of the TARP, we also examined the effect of a chimeric construct of γ-2 with the C-tail of the non-TARP γ-6 (γ-2/6; Fig. 4*A*). γ-2/6 behaved similarly to γ-2ΔC and produced less relief of polyamine block than did full-length γ-2 ($V_{½}$ of −43.4 ± 1.3 mV, $n = 6$; Fig. 4*B*). This suggests that the reduced relief of AMPAR polyamine block by γ-2ΔC is attributable to the absence of specific features within the C-tail. Finally, we coexpressed GluA1 with $\gamma\text{-}2_{(1-228)}$, a truncated form of γ-2 with a residual C-tail of similar length to γ-6 (Fig. 4*A*). $\gamma\text{-}2_{(1-228)}$ caused equivalent relief of polyamine block to full-length γ-2 and had a greater effect than both γ-2ΔC and γ-2/6 ($V_{½}$ of −31.4 ± 1.8 mV, $n = 5$; Fig. 4*B*). Together, these observations indicate that features within the membrane proximal region of the C-tail (specifically positions 207–228) are important mediators of this effect, albeit not its sole determinants.

TARP attenuation of polyamine block does not require GluA1 D586

Both calcium permeability and polyamine block of AMPARs depend critically on the neutral glutamine residue at the Q/R site. It has been shown that a neighboring conserved negatively charged aspartate residue (at the +4 position) is also a key determinant of polyamine block (Panchenko et al., 1999). Thus, replacing this with a neutral residue causes a marked reduction in rectification, although the channel remains calcium permeable (Dingledine et al., 1992; Panchenko et al., 1999). Because the specific sites that mediate TARP effects on AMPAR channel properties are not known, we examined the possibility that γ-2 might relieve polyamine block by altering the influence of the Q/R +4 negative aspartate.

We first confirmed that the +4 residue of GluA1 influenced polyamine block by replacing it with a neutral asparagine. As expected, with this GluA1(D586N) mutant, rectification was greatly decreased (Fig. 5). Next, we hypothesized that, if TARPs normally relieve AMPAR rectification by attenuating the influence of this charged residue, we would observe no change in rectification when GluA1(D586N) subunits were coexpressed with γ-2. This was not the case; rather, there was an additional attenuation of the polyamine block (Fig. 5). Similar results were seen with γ-3 and γ-5 (data not shown). Thus, TARP attenuation of polyamine block does not require the presence of GluA1 D586.

GluA1 D586 is crucial for TARP enhancement of single-channel conductance

GluA1 homomers expressed in the absence of TARPs have a relatively low single-channel conductance of ~20 pS (Suzuki et al., 2008; Coombs et al., 2012; Fig. 6). Strikingly, the D586N mutant decreased the single-channel conductance of GluA1 to approximately one-third of the wild-type value (from 19.7 ± 1.4 to 6.2 ± 0.6 pA; $n = 11$ and 10; Fig. 6*A*,*E*). Furthermore, the conductance of the mutant channel was no longer increased by coexpression with γ-2 or γ-3 (6.1 ± 0.7 and 7.3 ± 0.7 pS; $n = 8$ and 14; Fig. 6*B*,*E*). This lack of effect on conductance did not reflect a failure of coassembly, because both γ-2 and γ-3 slowed desensitization of GluA1(D586N), increasing $\tau_{w,des}$ from 3.8 ± 0.3 to 6.7 ± 0.4 and 7.0 ± 0.7 ms, respectively ($n = 10$, 8, and 14; Fig. 6*F*). Thus, the absence of a conserved negatively charged residue close to the Q/R site (D586N mutation in GluA1) not only decreased single-channel conductance but also prevented the conductance increase normally seen with TARP coexpression.

Because neutralizing D586 resulted in a loss of the TARP-mediated enhancement of GluA1 conductance, we reasoned that TARPs might increase channel conductance by promoting the influence of this negatively charged residue in the conduction pathway. If this were the case, then reversing the charge at this site

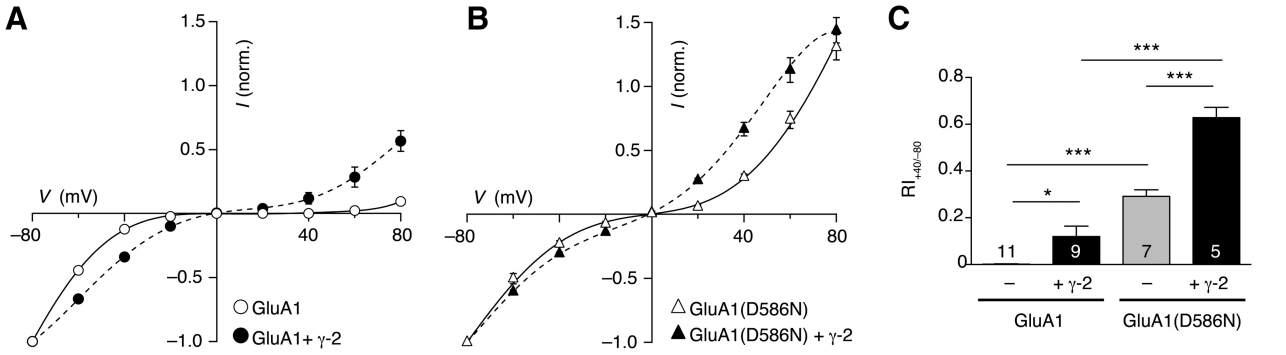

Figure 5. Neutralizing charge at the Q/R +4 position of GluA1(D586N) reduces polyamine block of CP-AMPARs but does not affect TARP-induced attenuation of block. ***A***, *I–V* relationships for glutamate-evoked peak responses (10 mM) between −80 and +80 mV in outside-out patches from cells expressing GluA1 homomers ($n = 11$) and GluA1 + γ-2 ($n = 9$). Symbols indicate the mean and error bars (when visible) ± SEM. ***B***, As for ***A*** but with GluA1(D586N) homomers ($n = 7$) and GluA1(D586N) + γ-2 ($n = 5$). ***C***, Pooled $RI_{+40/-80}$ values for GluA1 and GluA1(D586N) homomers alone and with γ-2. Mean values and SEM are shown; numbers in bars denote the number of patches. Two-way ANOVA revealed a significant main effect of AMPAR mutation ($F_{(1,28)} = 135.67$, $p < 0.001$), a significant main effect of TARP ($F_{(1,28)} = 32.68$, $p < 0.001$), and a significant interaction between AMPAR and TARP ($F_{(1,28)} = 8.88$, $p < 0.01$). *$p < 0.05$, ***$p < 0.001$, results of pairwise comparisons (unpaired Welch two-sample *t* tests with Holm's sequential Bonferroni correction).

might reverse the effect of TARPs on channel conductance. To test this, we examined the action of TARPs on another mutant, GluA1(D586K). As predicted, the introduction of a positively charged lysine at this site greatly decreased GluA1 conductance (to 4.3 ± 0.3 pS; $n = 10$; Fig. 6*C*,*E*). Moreover, coexpression of TARP γ-2 or γ-3 with the mutant receptor further reduced its conductance (to 2.2 ± 0.3 and 1.3 ± 0.4 pS, respectively; $n = 6$ and 4; Fig. 6*D*,*E*). Although the sign of TARP-induced conductance change was reversed with GluA1(D586K), both γ-2 and γ-3 produced the expected slowing of desensitization. Thus, $\tau_{w,des}$ was increased from 2.6 ± 0.2 to 4.1 ± 0.5 and 6.4 ± 1.0 ms, respectively ($n = 6$, 6, and 5; Fig. 6*F*). Furthermore, the steady-state current was increased from 1.3 ± 0.3 to 4.8 ± 0.8 and 6.5 ± 1.9%, suggesting a normal AMPAR–TARP functional interaction at the level of the ligand-binding domain (LBD). Together, these data reveal a novel site of TARP action that resides within the pore-lining region and is distinct from known TARP interactions with the LBD.

Discussion

Our experiments have provided three main findings. First, γ-2 modifies the permeation properties, although not the minimum pore diameter, of CP-AMPARs. Second, a proximal region of the γ-2 C-tail is involved in the TARP modulation of both channel conductance and polyamine block. Third, a negatively charged residue (D586), close to the Q/R site in the AMPAR pore lining, plays a crucial role in the TARP regulation of single-channel conductance. Below we consider the functional significance of these findings.

Influence of TARPs on channel permeability and pore size

We tested the idea that TARP domains might modify spermine block of CP-AMPARs by causing a change in the pore size (Milstein and Nicoll, 2008). Our comparison of TARPed and TARPless CP-AMPARs revealed that large ions (TMA^+, TEA^+, and $NMDG^+$) exhibit a TARP-induced increase in permeation. However, this did not translate into a measurable change in pore diameter.

The effect of TARPs on permeation and polyamine block may result from subtle changes in the pore architecture or in charge distribution in the region of the Q/R site that, together with neighboring residues, forms the selectivity filter and the narrowest constriction of the open pore (Kuner et al., 2001). Thus, even a small change in the positions of glutamine side chains in this region may greatly affect channel properties and disrupt key interactions involved in polyamine binding. This principle is clearly demonstrated by the effects of substituting other amino acids at this site (Burnashev et al., 1992), specifically the insertion of asparagine (N), which is found at the equivalent site (Q/R/N site) in NMDARs (Wollmuth and Sakmann, 1998). The asparagine side chain is one alkyl unit or ~1.5 Å shorter than glutamine but is otherwise chemically equivalent. Despite this relatively minor alteration, NMDARs and N-substituted AMPARs are insensitive to block by intracellular polyamines while remaining calcium permeable. Therefore, it is possible that the 20-fold decrease in polyamine affinity produced by γ-2 (Soto et al., 2007) reflects a minor change in position of the Q/R side chain.

Role of the C-tail of γ-2 in AMPAR function

Our experiments indicate that the C-tail of γ-2 plays a role in the relief of polyamine block of CP-AMPARs. We initially considered the possibility that three positively charged residues (Arg, His, and Lys) in the proximal region of the C-tail of γ-2 may influence this block. The auxiliary KAR subunits Neto1 and Neto2, which reduce polyamine block of GluK2(Q) KARs, have been shown to possess three positive charges in this region (Arg, Lys, Lys; +4 to 6 from the transmembrane domain) that are required for attenuation of polyamine block (Fisher and Mott, 2012). However, we observed no change in TARP attenuation of polyamine block when the homologous Arg, His, and Lys residues were neutralized in γ-2. Thus, there appears to be differences in how auxiliary subunits relieve polyamine block of CP-AMPARs versus KARs.

Although γ-2 was just as effective at attenuating polyamine block of GluA4 in the absence of three positively charged C-tail residues, it was markedly less effective after we deleted its entire C-terminal domain (γ-2ΔC). With this latter construct, polyamine block was intermediate between that of TARPed and TARPless CP-AMPARs, a feature that was mirrored by the γ-2/6 chimera. The less truncated form of the TARP ($\gamma\text{-}2_{(1-228)}$), which still lacked nearly 100 aa from its C-tail, behaved similarly to wild-type γ-2. Thus, features within the first 25 residues of the C-tail (proximal to M4) appear critical in modulating AMPAR channel properties. This would suggest that, if changes at the Q/R site are responsible for the TARP-induced relief of polyamine block, then the full expression of this effect depends in some way

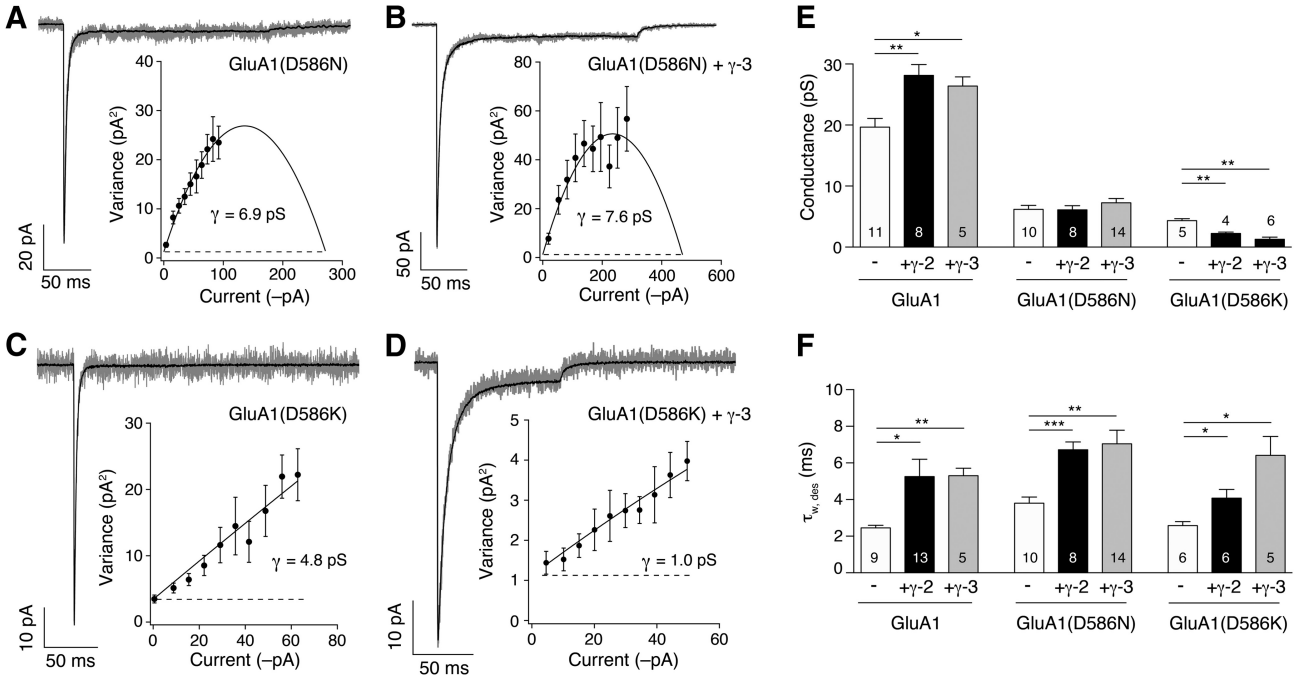

Figure 6. Mutations of GluA1 D586 alter both single-channel conductance and TARP modulation of conductance. ***A***, Currents elicited by rapid application of 10 mM glutamate (200 ms) to an outside-out patch from a tsA201 cell (−60 mV) transfected with GluA1(D586N). A single raw trace (gray) is shown overlaid with the mean response (black). The inset shows the current–variance plot for the same recording. The fitted parabola (see Materials and Methods) gave a weighted single-channel conductance of 6.9 pS. Dashed line denotes background variance, and error bars denote SEM. ***B***, Same as ***A*** but for a patch from a cell expressing GluA1(D586N) + γ-3, giving a weighted mean single-channel conductance of 7.6 pS. Note the slowed desensitization and increased steady-state current when compared with GluA1(D586N) alone. ***C***, Same as in ***A*** but a 100 ms application to a patch from a cell expressing GluA1(D586K), giving a weighted mean single-channel conductance of 4.8 pS. ***D***, Same as for ***C*** but for a patch from a cell expressing GluA1(D586K) + γ-3, giving a weighted mean single-channel conductance of 1.0 pS. Note the slowed desensitization and increased steady-state current compared with GluA1(D586K) alone. ***E***, Pooled data showing the effect of mutations D586N and D586K on the conductance of GluA1 and on the actions of TARPs γ-2 and γ-3. Mean values and SEM are shown; numbers in columns denote the number of patches. Two-way ANOVA revealed a significant main effect of AMPAR mutation ($F_{(2,62)} = 254.44$, $p < 0.001$), a significant main effect of TARPs ($F_{(2,62)} = 8.70$, $p < 0.001$), and a significant interaction between AMPAR and TARP ($F_{(4,62)} = 9.03$, $p < 0.001$). Pairwise comparisons for each of the GluA1 forms (unpaired Welch two-sample *t* tests with Holm's sequential Bonferroni correction) showed that TARPs γ-2 and γ-3 increased the conductance of GluA1, had no effect on the conductance of GluA1(D586N), but decreased the conductance of GluA1(D586K) (*$p < 0.05$, **$p < 0.01$). The conductance of both GluA1(D586N) and GluA1(D586K) was less than that of wild-type GluA1 ($^{###}p < 0.001$). ***F***, Pooled data showing the effect of mutations D586N and D586K on the actions of TARPs γ-2 and γ-3 on desensitization kinetics (presentation and tests as in ***E***). Two-way ANOVA revealed a significant main effect of AMPAR mutation ($F_{(2,65)} = 13.59$, $p < 0.001$), a significant main effect of TARPs ($F_{(2,65)} = 43.52$, $p < 0.001$), and no significant interaction between AMPAR and TARP ($F_{(4,65)} = 9.03$, $p = 0.38$). Pairwise comparisons for each of the GluA1 forms showed that TARPs γ-2 and γ-3 increased $\tau_{w,des}$ in all cases (*$p < 0.05$, **$p < 0.01$, ***$p < 0.001$).

on the proximal part of the C-tail of γ-2. The influence of this region could be transmitted through an effect on the tertiary structure of the TARP (intramolecular) or it could result from a direct interaction of the TARP C-tail with intracellular domains of the AMPAR (intermolecular). It should be noted that the reduction in attenuation of polyamine block by γ-2ΔC was less pronounced for GluA1 than for GluA4. While the reason for this is unclear, it may reflect differences between the C-tails of GluA1 and GluA4.

We found that γ-2 lacking its C-tail produced a greater increase in AMPAR mean channel conductance than did full-length γ-2. Single-channel studies have shown that AMPARs open to various distinct subconductance states (Wyllie et al., 1993; Swanson et al., 1997) thought to reflect the number of subunits individually activated (Rosenmund et al., 1998; Smith and Howe, 2000; Gebhardt and Cull-Candy, 2006). Thus, an increased mean conductance could reflect an increase in the proportion of openings to the larger subconductance states—altered gating—or an increase in the conductance of all states (altered permeation; Tomita et al., 2005; Shelley et al., 2012; Zhang et al., 2014). Our present data do not allow us to distinguish between these two possibilities. Interestingly, the former mechanism has been proposed to underlie the increase in AMPAR channel conductance caused by a different intracellular manipulation: phosphorylation of Ser831 in the C-tail of GluA1/GluA2 AMPARs, a functional change that is itself TARP dependent (Kristensen et al., 2011). By analogy, loss of the γ-2 C-tail could similarly enhance the ability of each subunit to activate, independent of changes in the efficacy of agonist-binding domain closure, thus increasing the likelihood that AMPAR subunits are simultaneously activated during gating. Clearly, it would be of interest to determine whether C-tail-lacking TARPs increase conductance of single-channel openings. However, regardless of the origin of our observed conductance changes, they suggest that, in addition to previously identified extracellular TARP structures (Tomita et al., 2005), intracellular components of the TARP molecule are important in regulating the ion channel.

GluA1 Asp586 is necessary for TARPs to enhance channel conductance

γ-2 relieved the polyamine block of wild-type and mutant (D586N) GluA1 to similar extents. Thus, it seems unlikely that any TARP influence on this residue is involved in attenuation of the block. However, Asp586 does appear critical in the TARP-induced increase in single-channel conductance. We found that the conductance of CP-AMPARs was greatly reduced when the negative aspartate (D) residue at the Q/R +4 site was replaced by a neutral asparagine (N) or a positively charged lysine (K). Fur-

thermore, the channel conductance of GluA1(D586N) was no longer increased by γ-2. Most strikingly, when the negative aspartate was replaced with a positive lysine (D586K), the channel conductance was decreased by coassembly with a TARP. Thus, it seems that the conserved negative charge at the Q/R +4 site (a glutamate residue in CP-KARs; Panchenko et al., 1999) is critical in determining both the conductance of AMPAR channels and the ability of TARPs to increase the conductance.

It is likely that the negatively charged Asp586 residue, situated on the inner vestibule of the AMPAR subunit, represents an important interaction point for positive ions in the conduction pathway, the removal of which decreases ion flux. Coexpression with a TARP could increase the effectiveness of D586 as a facilitator of ion transport, possibly by physically repositioning the charged side chain. Neutralizing or reversing the charge at this site has a striking effect on ion flux, decreasing the channel conductance and altering or reversing the effect of TARPs on channel conductance. Of note, we do not exclude the possibility that altered channel gating contributes to these changes; as with the effect of the TARP C-tail, detailed single-channel analysis could be informative. Interestingly, although we find a marked decrease in weighted mean channel conductance in receptors that lack this negatively charged residue, previous studies have shown that divalent permeability is not compromised (Dingledine et al., 1992; Panchenko et al., 1999).

That the channel conductance of GluA1(D586N) became insensitive to TARP coexpression was unexpected given that the TARP-induced relief of polyamine block of these mutant channels remained approximately comparable with that seen with wild-type GluA1. This suggests that TARPs can mediate effects through multiple sites within the pore, via both the Q/R site (influencing polyamine block) and the Q/R+4 site (influencing channel conductance). The crystal structure of GluA2 (Sobolevsky et al., 2009) suggests that gaps or grooves exist between the AMPAR transmembrane helices, potentially allowing residues from interacting TARPs to influence directly the AMPAR pore. Such intimate association could contribute to our observed alterations in AMPAR function, including the changes in permeation, ion channel conductance, and polyamine block.

References

Bats C, Soto D, Studniarczyk D, Farrant M, Cull-Candy SG (2012) Channel properties reveal differential expression of TARPed and TARPless AMPARs in *stargazer* neurons. Nat Neurosci 15:853–861. CrossRef Medline

Bowie D (2012) Redefining the classification of AMPA-selective ionotropic glutamate receptors. J Physiol 590:49–61. Medline

Burnashev N, Monyer H, Seeburg PH, Sakmann B (1992) Divalent ion permeability of AMPA receptor channels is dominated by the edited form of a single subunit. Neuron 8:189–198. CrossRef Medline

Burnashev N, Villarroel A, Sakmann B (1996) Dimensions and ion selectivity of recombinant AMPA and kainate receptor channels and their dependence on Q/R site residues. J Physiol 496:165–173. Medline

Chu PJ, Robertson HM, Best PM (2001) Calcium channel gamma subunits provide insights into the evolution of this gene family. Gene 280:37–48. CrossRef Medline

Cohen BN, Labarca C, Davidson N, Lester HA (1992) Mutations in M2 alter the selectivity of the mouse nicotinic acetylcholine receptor for organic and alkali metal cations. J Gen Physiol 100:373–400. CrossRef Medline

Coombs ID, Cull-Candy SG (2009) Transmembrane AMPA receptor regulatory proteins and AMPA receptor function in the cerebellum. Neuroscience 162:656–665. CrossRef Medline

Coombs ID, Soto D, Zonouzi M, Renzi M, Shelley C, Farrant M, Cull-Candy SG (2012) Cornichons modify channel properties of recombinant and glial AMPA receptors. J Neurosci 32:9796–9804. CrossRef Medline

Cull-Candy S, Kelly L, Farrant M (2006) Regulation of Ca^{2+}-permeable AMPA receptors: synaptic plasticity and beyond. Curr Opin Neurobiol 16:288–297. CrossRef Medline

Dingledine R, Hume RI, Heinemann SF (1992) Structural determinants of barium permeation and rectification in non-NMDA glutamate receptor channels. J Neurosci 12:4080–4087. Medline

Dwyer TM, Adams DJ, Hille B (1980) The permeability of the endplate channel to organic cations in frog muscle. J Gen Physiol 75:469–492. CrossRef Medline

Fisher JL, Mott DD (2012) The auxiliary subunits Neto1 and Neto2 reduce voltage-dependent inhibition of recombinant kainate receptors. J Neurosci 32:12928–12933. CrossRef Medline

Gebhardt C, Cull-Candy SG (2006) Influence of agonist concentration on AMPA and kainate channels in CA1 pyramidal cells in rat hippocampal slices. J Physiol 573:371–394. CrossRef Medline

Geiger JR, Melcher T, Koh DS, Sakmann B, Seeburg PH, Jonas P, Monyer H (1995) Relative abundance of subunit mRNAs determines gating and Ca^{2+} permeability of AMPA receptors in principal neurons and interneurons in rat CNS. Neuron 15:193–204. CrossRef Medline

Isaac JT, Ashby MC, McBain CJ (2007) The role of the GluR2 subunit in AMPA receptor function and synaptic plasticity. Neuron 54:859–871. CrossRef Medline

Jackson AC, Nicoll RA (2011) The expanding social network of ionotropic glutamate receptors: TARPs and other transmembrane auxiliary subunits. Neuron 70:178–199. CrossRef Medline

Jackson AC, Milstein AD, Soto D, Farrant M, Cull-Candy SG, Nicoll RA (2011) Probing TARP modulation of AMPA receptor conductance with polyamine toxins. J Neurosci 31:7511–7520. CrossRef Medline

Kott S, Sager C, Tapken D, Werner M, Hollmann M (2009) Comparative analysis of the pharmacology of GluR1 in complex with transmembrane AMPA receptor regulatory proteins g2, g3, g4, and g8. Neuroscience 158:78–88. CrossRef Medline

Kristensen AS, Jenkins MA, Banke TG, Schousboe A, Makino Y, Johnson RC, Huganir R, Traynelis SF (2011) Mechanism of Ca^{2+}/calmodulin-dependent kinase II regulation of AMPA receptor gating. Nat Neurosci 14:727–735. CrossRef Medline

Kuner T, Beck C, Sakmann B, Seeburg PH (2001) Channel-lining residues of the AMPA receptor M2 segment: structural environment of the Q/R site and identification of the selectivity filter. J Neurosci 21:4162–4172. Medline

Mähler J, Persson I (2012) A study of the hydration of the alkali metal ions in aqueous solution. Inorg Chem 51:425–438. CrossRef Medline

McKinnon NK, Reeves DC, Akabas MH (2011) 5-HT3 receptor ion size selectivity is a property of the transmembrane channel, not the cytoplasmic vestibule portals. J Gen Physiol 138:453–466. CrossRef Medline

Milstein AD, Nicoll RA (2008) Regulation of AMPA receptor gating and pharmacology by TARP auxiliary subunits. Trends Pharmacol Sci 29:333–339. CrossRef Medline

Nicoll RA, Tomita S, Bredt DS (2006) Auxiliary subunits assist AMPA-type glutamate receptors. Science 311:1253–1256. CrossRef Medline

Panchenko VA, Glasser CR, Partin KM, Mayer ML (1999) Amino acid substitutions in the pore of rat glutamate receptors at sites influencing block by polyamines. J Physiol 520:337–357. CrossRef Medline

Rosenmund C, Stern-Bach Y, Stevens CF (1998) The tetrameric structure of a glutamate receptor channel. Science 280:1596–1599. CrossRef Medline

Seeburg PH, Hartner J (2003) Regulation of ion channel/neurotransmitter receptor function by RNA editing. Curr Opin Neurobiol 13:279–283. CrossRef Medline

Shelley C, Farrant M, Cull-Candy SG (2012) TARP-associated AMPA receptors display an increased maximum channel conductance and multiple kinetically distinct open states. J Physiol 590:5723–5738. CrossRef Medline

Smith TC, Howe JR (2000) Concentration-dependent substate behavior of native AMPA receptors. Nat Neurosci 3:992–997. CrossRef Medline

Sobolevsky AI, Rosconi MP, Gouaux E (2009) X-ray structure, symmetry and mechanism of an AMPA-subtype glutamate receptor. Nature 462:745–756. CrossRef Medline

Soto D, Coombs ID, Kelly L, Farrant M, Cull-Candy SG (2007) Stargazin attenuates intracellular polyamine block of calcium-permeable AMPA receptors. Nat Neurosci 10:1260–1267. CrossRef Medline

Soto D, Coombs ID, Renzi M, Zonouzi M, Farrant M, Cull-Candy SG (2009) Selective regulation of long-form calcium-permeable AMPA receptors by an atypical TARP, gamma-5. Nat Neurosci 12:277–285. CrossRef Medline

Suzuki E, Kessler M, Arai AC (2008) The fast kinetics of AMPA GluR3 recep-

tors is selectively modulated by the TARPs gamma-4 and gamma-8. Mol Cell Neurosci 38:117–123. CrossRef Medline

Swanson GT, Kamboj SK, Cull-Candy SG (1997) Single-channel properties of recombinant AMPA receptors depend on RNA editing, splice variation, and subunit composition. J Neurosci 17:58–69. Medline

Tomita S, Adesnik H, Sekiguchi M, Zhang W, Wada K, Howe JR, Nicoll RA, Bredt DS (2005) Stargazin modulates AMPA receptor gating and trafficking by distinct domains. Nature 435:1052–1058. CrossRef Medline

Traynelis SF, Wollmuth LP, McBain CJ, Menniti FS, Vance KM, Ogden KK, Hansen KB, Yuan H, Myers SJ, Dingledine R (2010) Glutamate receptor ion channels: structure, regulation, and function. Pharmacol Rev 62:405–496. CrossRef Medline

Villarroel A, Burnashev N, Sakmann B (1995) Dimensions of the narrow portion of a recombinant NMDA receptor channel. Biophys J 68:866–875. Medline

Wollmuth LP, Sakmann B (1998) Different mechanisms of Ca^{2+} transport in NMDA and Ca^{2+}-permeable AMPA glutamate receptor channels. J Gen Physiol 112:623–636. CrossRef Medline

Wyllie DJ, Traynelis SF, Cull-Candy SG (1993) Evidence for more than one type of non-NMDA receptor in outside-out patches from cerebellar granule cells of the rat. J Physiol 463:193–226. Medline

Zhang W, Devi SP, Tomita S, Howe JR (2014) Auxiliary proteins promote modal gating of AMPA- and kainate-type glutamate receptors. Eur J Neurosci 39:1138–1147. CrossRef Medline